

Dynamic Coning Error Modeling Analysis of Laser Strapdown Inertial Navigation System

CHENG Guoda^{1,2*}, LIU Cong², GAO Guangen², WANG Shengjun², YAN Fei²

1. School of Automation, Northwestern Polytechnical University, Xi'an 710072, P. R. China;

2. AVIC Xi'an Flight Automatic Control Research Institute, Xi'an 710076, P. R. China

(Received 19 June 2023; revised 10 October 2023; accepted 15 November 2023)

Abstract: This paper proposes a modeling and compensation method for the dynamic coning error parameters of the mechanical dithered laser gyroscope. Firstly, the causes of the dynamic coning error are analyzed in principle, and the deformation of the sensing axis of the laser gyroscope under different external angular acceleration inputs is provided. A compensation model of the dynamic coning error is later established, and the influence of the dynamic coning error is represented by the dynamic coning error coefficient, which is only related to the laser gyro. Then we propose a system level calibration scheme of the dynamic coning error coefficients considering the relationship between the attitude error of the system before and after the coning motion. The existence of the dynamic coning error, as well as the dynamic coning error compensation effect is proved via the coning motion experiment of laser gyroscope and fiber optic gyroscope. Finally, it is verified through the system level vibration test that the dynamic coning error compensation method can effectively reduce the attitude and speed errors of the system in the vibration environment, consequently improving the navigation accuracy of the inertial navigation system in the complex mechanical environment.

Key words: mechanical dithered ring laser gyroscope; strapdown inertial navigation system; dynamic coning error; error model; parameter calibration

CLC number: TN925

Document code: A

Article ID: 1005-1120(2023)06-0641-12

0 Introduction

In recent years, the ring laser gyroscope (RLG) has become an ideal inertial component for strapdown inertial navigation systems (SINSs), which has been successfully used in many commercial and military navigation systems^[1-3]. The many advantages of RLG lie in its short start-up time, high reliability, long service life, wide dynamic range, good linearity, digital output, etc^[4-5]. In addition, RLG can provide angular velocity and acceleration information for flight control^[6] under satisfactory accuracy. SINS is directly connected with the aircraft, and inertial sensors directly reflect the movement of the aircraft. Therefore, the perfor-

mance of inertial sensors is supposed to meet with higher requirements.

Due to the existence of backscattering and non-uniform loss in RLG, the clock wise (CW) and counterclock wise (CCW) laser beams in the RLG cavity are synchronized^[7-9] when the external input angular rate is lower than a certain threshold. The RLG enters the lock-in region correspondingly. In order to eliminate the effect of the lock-in problem and improve the performance of the laser gyroscope, frequency offset measures are adopted, of which mechanical dithering is one of the most commonly used methods^[10-13].

Mechanical dithering applies angular vibrations to the entire cavity at high frequency, low amplitude

*Corresponding author, E-mail address: dhhbgd@mail.nwpu.edu.cn.

How to cite this article: CHENG Guoda, LIU Cong, GAO Guangen, et al. Dynamic coning error modeling analysis of laser strapdown inertial navigation system[J]. Transactions of Nanjing University of Aeronautics and Astronautics, 2023, 40(6): 641-652.

<http://dx.doi.org/10.16356/j.1005-1120.2023.06.002>

and small angles to avoid low-frequency outputs^[14]. However, the coupling among the three-axis gyroscopes in the laser SINS would cause the coning motion^[15] of the entire platform. Under such circumstances, the input of external acceleration could cause the flexure errors^[16-17] of the dithering axis, which might bring distinct gyro drift to the navigation system^[18] eventually.

The environment could be very harsh and the mechanical environment is complex in many applications, especially in the military field. The mechanical parts in the mechanical dithered laser gyroscope^[19] are dynamic, which seriously affects the anti-vibration performance of the dithered laser gyroscope, consequently restricting the application of the dithered laser gyroscope. Therefore, it is of great necessity to study the inner mechanism affecting the vibration characteristics of mechanically dithered laser gyroscopes, and to provide effective measures for improving the vibration performance of the gyroscope^[20].

Despite suitable vibration reduction structures are designed to reduce the impact of vibration on the laser SINS, the precision of the inertial navigation system in the vibration environment still declines rapidly. The existence of the mechanically dithered laser gyroscope mechanism^[21] could bend the dithering axis under the action of acceleration, resulting in an equivalent installation error, which in turn produces an equivalent gyro drift. Ref.[22] theoretically deduced the drift error caused by the bending deformation of the dithering axis of the mechanically dithered laser gyroscope^[23]. It assumes that the error is proportional to the input acceleration and the dynamic frequency of the system, and verifies the assumption through simulation. But there still lack of further experimental verification and error compensation methods. As far as we are concerned, there are few published literatures about the analysis and compensation scheme of the dynamic offset error model of the sensitive axis of the mechanically dithered laser gyroscope.

The laser gyroscope dynamic coning error denotes the precision of the laser inertial navigation dropping significantly under certain complex me-

chanical environment. In a complex mechanical environment, the coning motion occurs due to two forms of coupling, the coupling of external angular motion, and the linear and angular coupling of the inertial navigation system vibration reduction system^[24-27]. The coning motion is coupled with the external acceleration, resulting in a conical offset of the sensitive axis of the mechanically dithered laser gyroscope. Consequently, the coning motion brings the equivalent gyroscope drift error, which causes the precision of the laser inertial navigation to drop significantly, namely the laser gyroscope dynamic coning error.

In this paper, a compensation model for the dynamic coning error parameters of mechanical dithered laser gyroscope is proposed. First we analyze the causes of the dynamic coning error in principle by implementing the finite element analysis method. The compensation model of the dynamic coning error is established, and a system level calibration scheme of the dynamic coning error coefficients is designed. Then the existence of the dynamic coning error has been verified via the coning motion experiment of laser gyroscope and fiber optic gyroscope. The dynamic coning error compensation effect is first proved via the system level coning motion experiment. Through the system level vibration test, it is verified that the proposed dynamic coning error compensation method can effectively improve the navigation accuracy of the inertial navigation system in the complex mechanical environment.

1 Dynamic Coning Error Modeling and Compensation

1.1 Modeling of dynamic coning error

The coning movement occurs when the angular vibrations of the gyroscope are of the same frequency and different phases on its rotation axis and output axis. In this case, although the direction of the input axis remains unchanged, the gyroscope is sensitive to the input axis, resulting in a constant angular rate signal output. The angular velocity of movement of the gyro mount can be described as^[26]

$$\boldsymbol{\omega}(t) = [a\Omega \sin(\Omega t) \quad b\Omega \cos(\Omega t) \quad c]^T \quad (1)$$

where a , b and c are all constants, $\boldsymbol{\omega}(t)$ represents angular velocity, t the duration of time, and Ω the vibration frequency on x and y axes of the sinusoidal angular vibration with the same frequency and phase difference of 90° , while the angular velocity of z -axis remains constant.

According to the quaternion differential equation, the angular velocity can be obtained as

$$\boldsymbol{\omega}(t) = \begin{bmatrix} -\Omega \sin\phi \sin(\Omega t) \\ \Omega \sin\phi \cos(\Omega t) \\ -2\Omega \sin^2(\phi/2) \end{bmatrix} \quad (2)$$

It can be seen from Eq.(2) that when there are sinusoidal angular vibrations of the same frequency but with a phase difference of 90° in x and y axes, there will be a constant angular motion of $c = -2\Omega \sin^2(\phi/2)$ on the z axis. In this case, the z axis draws a conical surface in space, and the semi-cone angle is ϕ .

The above form of coning motion is obtained under the premise that the entire gyroscope is regarded as a rigid body. The coning motion would cause the gyroscope an equivalent gyroscope drift, and there are many compensation methods aiming for this part of the error^[28-31]. However, the laser sensor of the mechanical dithering laser gyroscope is directly fixed to the bottom shell through the dithering mechanism at the center. Taking the z -axis gyroscope as an example, when there is horizontal vibration in the x and y directions, lateral torsion angle vibration will inevitably occur, which will cause a certain degree of dynamic offset error to the sensitive axis of the gyroscope.

As shown in Fig.1, when the gyroscope is in coning motion, there is angular acceleration input and the sensitive axis of the gyroscope will produce a conical offset. In Fig.1, $\dot{\omega}_x$, $\dot{\omega}_y$, and $\dot{\omega}_z$ are angular accelerations of x , y and z axes, respectively, $\dot{\omega}_d$ and $\dot{\omega}_r$ are the dithering acceleration amplitude of laser gyro and the external input angular acceleration amplitude, respectively, and f_d and f_r are the dithering frequency of laser gyro and the external input angular acceleration frequency, respectively. As a result, the precision of the laser inertial navigation

would drop significantly under the complex mechanical environment. The existence of the gyroscope sensitive axis offset hinders the previous coning error compensation algorithm from complete compensation of the gyroscope drift. Under the premise of ignoring the non-commutative error, in this paper the residual error of the coning motion caused by the offset of the gyroscope sensitive axis is referred as the dynamic coning error.

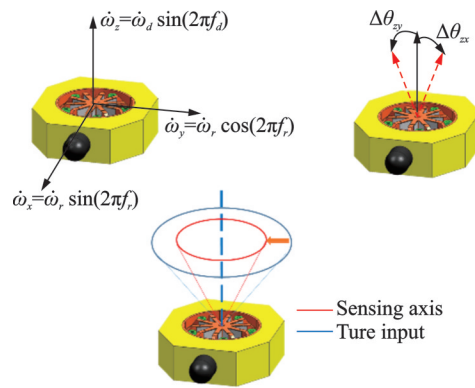


Fig.1 Laser gyroscope sensitive axis coning offset

Taking the z -axis gyro as the research object, under complex external mechanical environment, there will be an angular acceleration along the x and y directions in addition to coning motion. Under the assumption of small deformation, the inertia moments in the x and y directions are as

$$M_{zx} = J_{zx} \alpha_{zx}, \quad M_{zy} = J_{zy} \alpha_{zy} \quad (3)$$

where J_{zx} and J_{zy} are the moments of inertia of the z -gyroscope around the x and y axes; and α_{zx} and α_{zy} the angular accelerations of the z -gyroscope around the x and y axes, respectively. The lateral stiffness of the same gyro in different directions is very close, and the influence of anisotropy is safely to ignore. Under the same assumption of small deformation, the small deformation angle caused by the angular acceleration of the gyro is expressed as

$$\Delta\theta_{zx} = \frac{M_{zx}}{k_z}, \quad \Delta\theta_{zy} = \frac{M_{zy}}{k_z} \quad (4)$$

where k_z is the lateral stiffness.

In order to verify the influence of angular acceleration on gyroscope sensitive axis offset, we establish a model of the laser gyroscope and carry out finite element simulation. The definition of the axis of the laser gyro is shown in Fig.2.

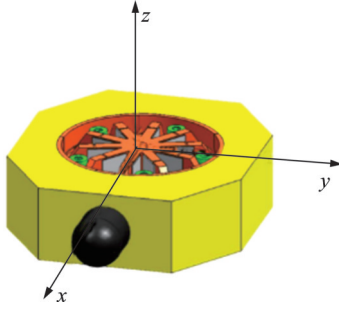


Fig.2 Definition of laser gyroscope coordinate axis

We then apply constant angular acceleration to the gyroscope along the x axis and y axis respectively, and simulate the deflection angle of the measuring point on the sensitive axis under different angular accelerations. Fig.3 is the finite element simulation diagrams of the laser gyroscope with the angular acceleration on the x and y directions. Point O is the fixed point at the bottom center of the laser gyroscope housing. The displacement and deflection angle of point A and point B on the sensitive axis are measured through simulation. The measurement results are shown in Table 1 and Table 2.

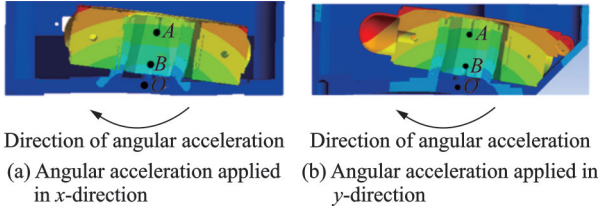


Fig.3 Finite element simulation diagram of laser gyroscope

Table 1 Displacement and deflection angle of the laser gyroscope sensitive axis when the angular acceleration applied in x direction

Angular acceleration/ ($\text{rad}\cdot\text{s}^{-2}$)	100	200	500	1 000
Displacement of $A/\mu\text{m}$	0.137 2	0.274 3	0.685 8	1.371 5
Displacement of $B/\mu\text{m}$	0.091 6	0.183 2	0.458 0	0.916 0
Deflection angle of $A/\mu\text{rad}$	6.73	13.46	33.65	67.30
Deflection angle of $B/\mu\text{rad}$	13.63	27.26	68.15	136.30

Table 2 Displacement and deflection angle of the laser gyroscope sensitive axis when the angular acceleration applied in y direction

Angular acceleration/ ($\text{rad}\cdot\text{s}^{-2}$)	100	200	500	1 000
Displacement of $A/\mu\text{m}$	0.153 9	0.307 8	0.769 6	1.539 2
Displacement of $B/\mu\text{rad}$	0.100 9	0.201 9	0.504 7	1.009 5
Deflection angle of $A/\mu\text{rad}$	7.55	15.10	37.75	75.51
Deflection angle of $B/\mu\text{rad}$	15.02	30.04	75.09	150.19

As the external angular acceleration increases, the displacement and deflection angle of the measuring point on the sensitive axis of the laser gyroscope increase synchronously. Although the deformation of gyroscope is very small, it can not be ignored in the study of the high dynamic motion of high-precision gyroscope.

It is necessary to consider the influence of the small deformation on the coning motion when studying the coning motion of high-precision gyroscopes. As shown in Fig.1, the influence can be regarded as the conical offset of the sensitive axis of the gyroscope, resulting in an additional equivalent coning error. Combining Eqs.(3) and (4), it can be deduced that

$$\begin{cases} \Delta\theta_{zx} = \frac{J_{zx}}{k_z} \alpha_{zx} = K_{zx} \alpha_{zx} = K_{zx} \ddot{\theta}_x \\ \Delta\theta_{zy} = \frac{J_{zy}}{k_z} \alpha_{zy} = K_{zy} \alpha_{zy} = K_{zy} \ddot{\theta}_y \end{cases} \quad (5)$$

where K_{zx} and K_{zy} denote the dynamic coning error coefficients, which only depend on the size of the gyroscope, the installation position, and the gyroscope stiffness. It can be represented through certain calibration compensation methods. The moment inertia of the gyroscope is calculated by software, and the coning error coefficient can be further estimated approximately to be $7.9\text{e}-8$. The deformation angle calculated by substituting Eq.(5) is roughly as the value in Table 1. $\ddot{\theta}_x$ and $\ddot{\theta}_y$ represent the angular acceleration of the inertial navigation system along the x and y axes, which can represent the z gyro angular acceleration and can be measured in real time.

In the same way, the dynamic gyro coning motion error coefficients and angular acceleration of the x and y gyroscopes can be obtained. In this paper, the small angle error of the above-mentioned gyro sensitive axis is equivalent to the gyro installation declination angle for compensation. The compensation formula is as follows

$$\begin{cases} \epsilon_{xy} = \epsilon_{xy0} - \Delta\theta_{xy} = \epsilon_{xy0} - K_{xy} \ddot{\theta}_y \\ \epsilon_{xz} = \epsilon_{xz0} - \Delta\theta_{xz} = \epsilon_{xz0} - K_{xz} \ddot{\theta}_z \\ \epsilon_{yx} = \epsilon_{yx0} - \Delta\theta_{yx} = \epsilon_{yx0} - K_{yx} \ddot{\theta}_x \\ \epsilon_{yz} = \epsilon_{yz0} - \Delta\theta_{yz} = \epsilon_{yz0} - K_{yz} \ddot{\theta}_z \\ \epsilon_{zx} = \epsilon_{zx0} - \Delta\theta_{zx} = \epsilon_{zx0} - K_{zx} \ddot{\theta}_x \\ \epsilon_{zy} = \epsilon_{zy0} - \Delta\theta_{zy} = \epsilon_{zy0} - K_{zy} \ddot{\theta}_y \end{cases} \quad (6)$$

Taking the first formula in Eq.(6) as an example, ϵ_{xy0} denotes the initial installation declination offset angle of the x -axis gyro around the y -axis direction. The meanings of variables in other formula in Eq.(6) are defined in the similar way respectively.

The error compensation model of the gyroscope in the actual inertial measurement unit is as follows

$$\begin{bmatrix} \omega_{ibx}^b \\ \omega_{iby}^b \\ \omega_{ibz}^b \end{bmatrix} = \begin{bmatrix} 1 & \epsilon_{xz} & \epsilon_{xy} \\ \epsilon_{yz} & 1 & \epsilon_{yx} \\ \epsilon_{zy} & \epsilon_{zx} & 1 \end{bmatrix} \begin{bmatrix} (1 - \delta k_{gxx}) \omega_{ibx}^{b_x} - \epsilon_x^{b_x} \\ (1 - \delta k_{gyy}) \omega_{iby}^{b_y} - \epsilon_y^{b_y} \\ (1 - \delta k_{gzz}) \omega_{ibz}^{b_z} - \epsilon_z^{b_z} \end{bmatrix} \quad (7)$$

In Eq.(7), the non cartesian coordinate system of the gyroscope sensitive axis is denoted as the b_g coordinate system. δk_{gii} ($i = x, y, z$) is the gyro scale coefficient error, and $\epsilon_i^{b_x}$ is the zero drift error. The traditional gyro error compensation formula is as Eq.(7). After adding dynamic coning error compensation, the gyro installation deviation compensation value is updated via Eq.(6) in practical applications.

1.2 Calibration method of dynamic coning error

The relation between the cone offset angle and the angular acceleration of the laser gyroscope in the complex mechanical environment is analyzed in the previous section. The dynamic coning error coefficient of the laser gyroscope has been introduced for the quantitative description in this section. As mentioned above, the dynamic coning error coefficient of the gyroscope only depends on the size, installation position and stiffness of the gyroscope itself, which can be compensated in real time through prior calibration. In this section, a scheme for calibrating the dynamic coning error coefficients of laser gyroscope is proposed. Within certain navigation time, the dynamic coning error could cause additional attitude error of the inertial navigation system. This section establishes the relation between the dynamic coning error and attitude error of the inertial navigation system, and employs the calibration process by deriving the dynamic coning error coefficient from the attitude error solved by the inertial navigation system under certain motion condition.

This paper uses a three-axis turntable to apply

coning motion to the calibrated system, and an angular acceleration input is introduced to excite the dynamic coning error of the system. By controlling the two axes of the turntable to make a sinusoidal motion with a phase difference of 90° , a conical motion with a semi-cone angle of ϕ and a cone frequency of Ω is generated on the third axis. IMU coordinate system is defined as the b system, geographic coordinate system is the n system, and the initial position of inertial navigation system is the n_0 system. Taking the coning motion generated by the system on axis x as an example, the angular velocity input of each axis of IMU is as

$$\omega_b(t) = \begin{bmatrix} 2\Omega \sin^2\left(\frac{\phi}{2}\right) \\ \Omega \sin\phi \cos(\Omega t) \\ -\Omega \sin\phi \sin(\Omega t) \end{bmatrix} \quad (8)$$

Under the assumption of small angle cone motion, the angular velocity input can be simplified as

$$\omega_b(t) = \begin{bmatrix} \frac{\Omega\phi^2}{2} \\ \Omega\phi \cos(\Omega t) \\ -\Omega\phi \sin(\Omega t) \end{bmatrix} \quad (9)$$

The angular acceleration is

$$\dot{\omega}_b(t) = \begin{bmatrix} 0 \\ -\Omega^2\phi \sin(\Omega t) \\ -\Omega^2\phi \cos(\Omega t) \end{bmatrix} \quad (10)$$

The coordinate deviation angle of b system relative to n_0 system is

$$\theta_x = 0; \theta_y = \phi \sin(\Omega t); \theta_z = \phi \cos(\Omega t) \quad (11)$$

Under the premise that the deviation angle of b system relative to n_0 system is small, the transformation matrix from n_0 system to b system is as

$$C_{n_0}^b(t) = \begin{bmatrix} 1 & \theta_z & -\theta_y \\ -\theta_z & 1 & \theta_x \\ \theta_y & -\theta_x & 1 \end{bmatrix} \quad (12)$$

where t denotes the time of coning motion.

At this position, when n_0 system and n system coincide (if the initial position changes, there is a corresponding coordinate transformation matrix), we have

$$C_{n_0}^n(t) = \begin{bmatrix} 1 & 0 & 0 \\ 0 & 1 & 0 \\ 0 & 0 & 1 \end{bmatrix} \quad (13)$$

$$\mathbf{C}_b^n(t) = \mathbf{C}_{n_0}^n(t) \mathbf{C}_b^{n_0}(t) = \begin{bmatrix} 1 & -\phi \cos(\Omega t) & \phi \sin(\Omega t) \\ \phi \cos(\Omega t) & 1 & 0 \\ -\phi \sin(\Omega t) & 0 & 1 \end{bmatrix} \quad (14)$$

Considering that the system angular acceleration due to the coning motion could cause the dynamic coning error, the actual equivalent installation

$$\delta \boldsymbol{\omega}_n(t) = \mathbf{C}_b^n(t) \begin{bmatrix} 0 & \boldsymbol{\varepsilon}_{xz}(t) & \boldsymbol{\varepsilon}_{xy}(t) \\ \boldsymbol{\varepsilon}_{yz}(t) & 0 & \boldsymbol{\varepsilon}_{yx}(t) \\ \boldsymbol{\varepsilon}_{zy}(t) & \boldsymbol{\varepsilon}_{zx}(t) & 0 \end{bmatrix} \boldsymbol{\omega}_b(t) =$$

$$\begin{bmatrix} 1 & -\phi \cos(\Omega t) & \phi \sin(\Omega t) \\ \phi \cos(\Omega t) & 1 & 0 \\ -\phi \sin(\Omega t) & 0 & 1 \end{bmatrix} \begin{bmatrix} 0 & \boldsymbol{\varepsilon}_{xz}(t) & \boldsymbol{\varepsilon}_{xy}(t) \\ \boldsymbol{\varepsilon}_{yz}(t) & 0 & \boldsymbol{\varepsilon}_{yx}(t) \\ \boldsymbol{\varepsilon}_{zy}(t) & \boldsymbol{\varepsilon}_{zx}(t) & 0 \end{bmatrix} \begin{bmatrix} \frac{\Omega \phi^2}{2} \\ \Omega \phi \cos(\Omega t) \\ -\Omega \phi \sin(\Omega t) \end{bmatrix} =$$

$$\begin{bmatrix} -\phi \cos(\Omega t) \boldsymbol{\varepsilon}_{yz}(t) + \phi \sin(\Omega t) \boldsymbol{\varepsilon}_{zy}(t) & \boldsymbol{\varepsilon}_{xz}(t) + \phi \sin(\Omega t) \boldsymbol{\varepsilon}_{zx}(t) & \boldsymbol{\varepsilon}_{xy}(t) - \phi \cos(\Omega t) \boldsymbol{\varepsilon}_{yx}(t) \\ \boldsymbol{\varepsilon}_{yz}(t) & \phi \cos(\Omega t) \boldsymbol{\varepsilon}_{xz}(t) & \phi \cos(\Omega t) \boldsymbol{\varepsilon}_{xy}(t) + \boldsymbol{\varepsilon}_{yx}(t) \\ \boldsymbol{\varepsilon}_{zy}(t) & -\phi \sin(\Omega t) \boldsymbol{\varepsilon}_{xz}(t) + \boldsymbol{\varepsilon}_{zx}(t) & -\phi \sin(\Omega t) \boldsymbol{\varepsilon}_{xy}(t) \end{bmatrix} \begin{bmatrix} \frac{\Omega \phi^2}{2} \\ \Omega \phi \cos(\Omega t) \\ -\Omega \phi \sin(\Omega t) \end{bmatrix} \quad (16)$$

Under the premise of small angle assumption within certain period, ignoring the high-order terms in Eq.(16) and the terms whose integral is zero in the positive integration period, the simplification is obtained as

$$\frac{\delta \bar{\boldsymbol{\omega}}_n(t)}{\boldsymbol{\omega}_z} = \begin{bmatrix} \frac{\phi^2}{2} K_{yz} - \frac{\phi^2}{2} K_{zy} - K_{xz} + K_{xy} \\ \boldsymbol{\varepsilon}_{yz0} + \boldsymbol{\varepsilon}_{xz0} \\ \boldsymbol{\varepsilon}_{zy0} - \boldsymbol{\varepsilon}_{xy0} \end{bmatrix} \quad (17)$$

The left side of Eq.(17) can be calculated using the attitude error before and after the cone motion. The right side contains some dynamic coning motion error coefficients. By coning at multiple positions, we can obtain the conversion relations among all dynamic coning error coefficients and attitude errors, and then calibrate the dynamic coning error coefficients. In the practical compensation process, the dynamic coning error is compensated by measuring the angular acceleration of the system and calculating the equivalent installation deflection angle in real time.

The dynamic coning motion error calibration experiment is carried out for a laser inertial navigation system with an accuracy of 0.8 nmile/h, and

tion deflection angle is as follows

$$\begin{cases} \boldsymbol{\varepsilon}_{xy}(t) = \boldsymbol{\varepsilon}_{xy0} - K_{xy} \Omega^2 \phi \sin(\Omega t) \\ \boldsymbol{\varepsilon}_{xz}(t) = \boldsymbol{\varepsilon}_{xz0} - K_{xz} \Omega^2 \phi \cos(\Omega t) \\ \boldsymbol{\varepsilon}_{yx}(t) = \boldsymbol{\varepsilon}_{yx0} \\ \boldsymbol{\varepsilon}_{yz}(t) = \boldsymbol{\varepsilon}_{yz0} - K_{yz} \Omega^2 \phi \cos(\Omega t) \\ \boldsymbol{\varepsilon}_{zx}(t) = \boldsymbol{\varepsilon}_{zx0} \\ \boldsymbol{\varepsilon}_{zy}(t) = \boldsymbol{\varepsilon}_{zy0} - K_{zy} \Omega^2 \phi \cos(\Omega t) \end{cases} \quad (15)$$

Angular rate error in geographical system is

the calibration results are shown in Table 3. The order of magnitude of the results in the table is equivalent to the modeling results above.

Table 3 Calibration results of the dynamic coning error coefficient

Coefficient	Value	Coefficient	Value
K_{xy}	6.9e-8	K_{yz}	7.3e-8
K_{xz}	7.1e-8	K_{zx}	6.7e-8
K_{yx}	7.5e-8	K_{zy}	7.6e-8

2 Verification of Dynamic Coning Error Effect

2.1 Verification of RLG

In order to verify the existence of the dynamic coning error of the mechanically dithered laser gyroscope, in this section, we conduct a comparative experiment with the laser gyroscope and the optical fiber gyroscope of the same precision. We install two systems in the symmetrical position of the dual-axis turntable, and control the two axes of the turntable to perform the same-frequency sinusoidal motion

with a phase difference of 90° to ensure the same coning motion on the gyroscopes.

First, we let the rotary axis of the turntable perform a small-amplitude angular movement of 15 Hz, and record the output of the gyroscopes as shown in Fig.4. The two curves in Fig.4 represent the change of the output value of the laser gyroscope and the fiber optic gyroscope over time respectively. The output has been subtracted off the average angular velocity the gyroscope sensitive to when the gyroscope is stationary.

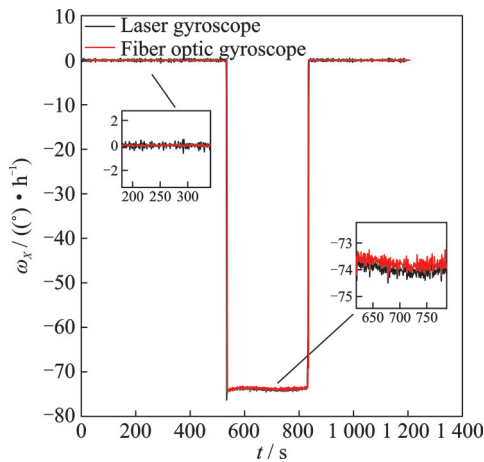


Fig.4 Gyroscope output curves of 15 Hz coning motion

The time range where the curve value is 0 denotes that the turntable is stationary, and the range with the step output value denotes the turntable moving and producing a coning motion on the sensitive axis of the gyroscope. It can be seen from the enlarged graph of the curve that the outputs of the laser gyroscope and the fiber optic gyroscope are relatively coincident in the stationary part; while in the coning motion part, there is a relatively obvious difference between the two curves.

The average output difference between the two gyroscopes in the coning motion stage is calculated around $0.5^\circ/\text{h}$, which is an unacceptable error for a high-precision gyroscope. It can be concluded from the movement of the turntable that the angular velocity input brought by the coning motion is in good coincidence with the fiber optic gyroscope. Hence, it can be deduced that the output error of the laser gyroscope under the coning motion is caused by the dynamic coning error analyzed in the previous section.

Then we set the turntable perform angular motion with a larger amplitude of 1 Hz, and record the gyroscope output of the two gyroscopes as shown in Fig.5. It can be seen that in the stationary stage of the turntable, the outputs of the laser gyroscope and the fiber optic gyroscope are relatively coincident. In the coning motion stage, although the angular velocity input brought by the coning motion is relatively large, the output of the two gyroscope is still consistent.

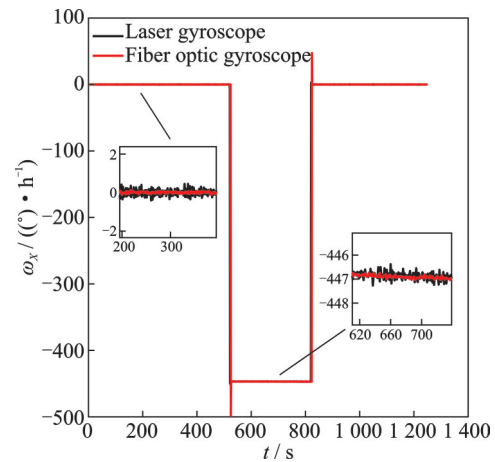


Fig.5 Gyroscope output curves of 1 Hz coning motion

The experiments show that the cone angle of the coning motion is not the key factor causing the dynamic coning error. Even if it brings a relatively large angular velocity input, the dynamic coning error of the laser gyroscope is limited. On the other hand, when the frequency of the coning motion is accelerated, even a small angular velocity input will bring about a very obvious dynamic coning error, which is consistent with the analysis conclusion in the previous section. The angular acceleration is the cause of the deformation of the sensitive axis of the gyroscope, which in turn brings about the dynamic coning error.

2.2 Verification of SINS

In this section, to verify the influence of dynamic coning error on the navigation accuracy of the system, we implement the coning test using laser strapdown inertial navigation system and optical fiber strapdown inertial navigation system with the same accuracy level. The standard strapdown inertial navigation system used for this test is with navigation accuracy of 0.8 nmile/h .

Under the coning motion frequency of 15 Hz, the attitude change curves of the two systems are shown in Fig.6, of which three subgraphs represent the change curves of pitch, roll and heading angle respectively. The attitude step change part in the figure represents that the turntable starts coning motion. It can be seen from the figure that under the high-frequency coning motion, due to the obvious dynamic coning error effect, the pitch axis of the laser inertial navigation system produces significant attitude error before and after the coning motion, while the attitude error of the optical fiber system before and after the coning motion is relatively small.

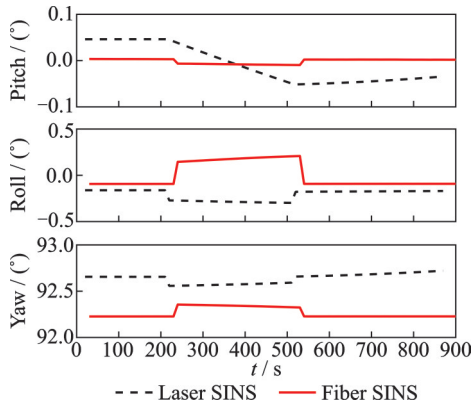


Fig.6 Attitude change curves of 15 Hz coning motion with two systems

The velocity curves of the two systems are shown in Fig.7, where V_e and V_n are the east and north velocities, respectively. It can be seen that the attitude error of the laser inertial navigation system caused by the dynamic coning motion error causes

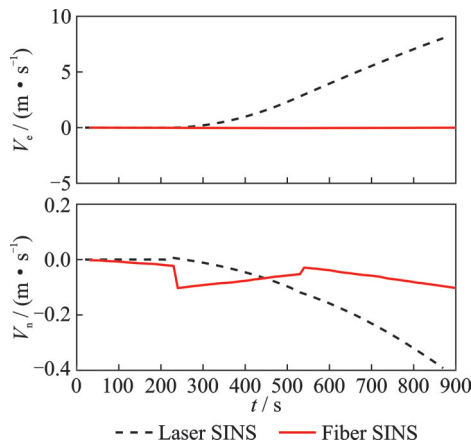


Fig.7 Velocity change curves of 15 Hz coning motion with two systems

its east velocity to diverge rapidly, and the navigation error of the laser inertial navigation system increases rapidly.

The same coning motion test is carried out after calibrating and compensating the dynamic coning error parameters of the laser inertial navigation system. Fig.8 shows the attitude change curves of the system before and after compensation. It can be seen from the figure that the attitude error of the pitch axis is significantly reduced. Fig.9 shows the velocity change curves of the system before and after the compensation. It can be seen from the figure that the velocity error of the system also decreases significantly after the dynamic coning error is compensated. The above experimental results verify the effectiveness of the proposed dynamic coning error compensation scheme.

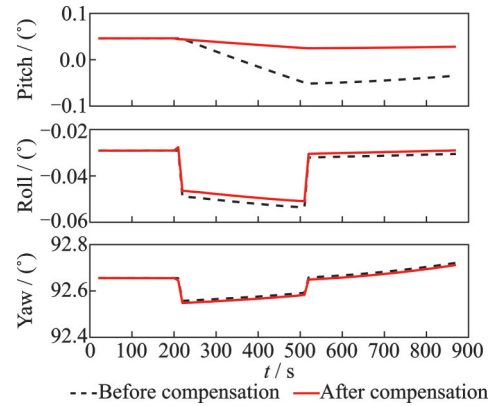


Fig.8 Attitude change curves of SINS before and after dynamic coning motion error compensation under 15 Hz coning motion

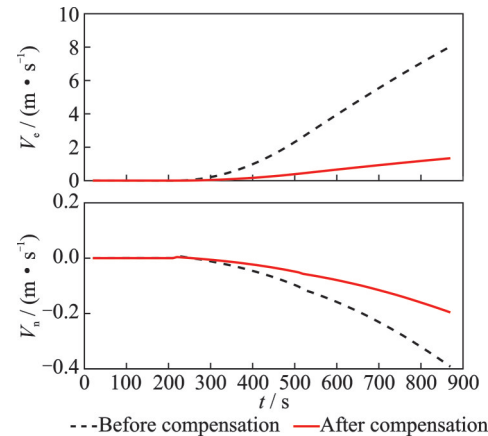


Fig.9 Velocity change curves of SINS before and after dynamic coning motion error compensation under 15 Hz coning motion

3 System-Level Experiment of Dynamic Coning Error Compensation

In order to further verify the validity of the proposed dynamic coning error model, and to verify that it can improve the system performance in a complex mechanical environment, we calibrate the dynamic coning error of a laser SINS used above and perform a vibration test. During the test, the original IMU measurement data of 4 000 Hz frequency are also stored for offline compensation comparison experiment. A long-time vibration test has been carried out on the laser SINS in the x and y directions using the vibration spectrum of a relatively large energy level, and the test results before and after compensation under the same test conditions are obtained respectively.

The curves in Figs.10 and 11 denote the changes of the attitude output of the inertial navigation system over time under the vibration in the x and y directions respectively. The three subplots represent pitch, roll, and yaw angle changes respectively. It can be seen from Table 4 that regardless of the vibration direction, during and after the vibration process, the attitude error of the system after dynamic coning error compensation is significantly smaller than that of the uncompensated system.

Due to the offset of the sensitive axis of the laser gyroscope caused by the vibration environment, the equivalent coning error cannot be ignored, resulting in a significant jump in the system attitude output before and after the vibration. After compen-

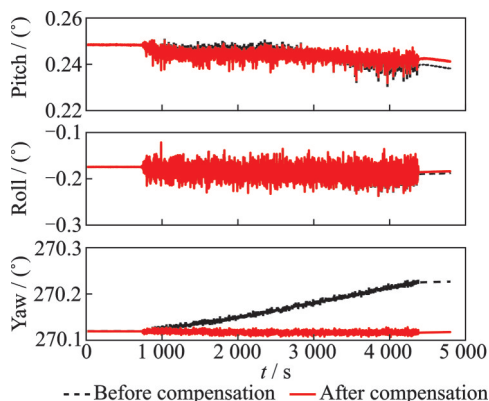


Fig.10 Attitude error curves under x -direction vibration

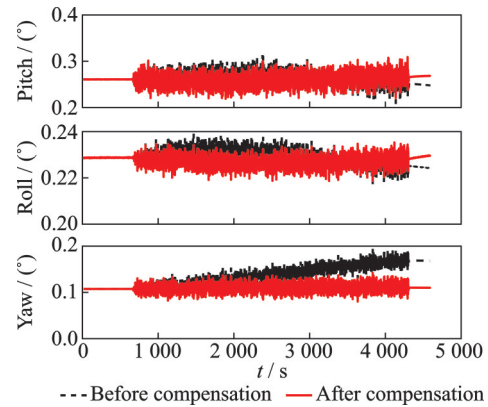


Fig.11 Attitude error curves under y -direction vibration

Table 4 Comparison of attitude errors before and after vibration

Attitude	Attitude error before compensation / (°)	Attitude error after compensation / (°)	Reduction / %
Pitch(x -direction vibration)	0.003 8	0.001 5	60.53
Roll(x -direction vibration)	0.012	0.008	33.33
Yaw(x -direction vibration)	0.10	0.001 8	98.20
Pitch(y -direction vibration)	0.021	0.015	28.57
Roll(y -direction vibration)	0.002 4	0.001 0	58.33
Yaw(y -direction vibration)	0.062	0.011	82.26

sating the dynamic coning error, the output attitude consistency before and after the system vibration improves, which proves that the dynamic coning error modeling compensation method proposed in this paper can effectively decrease the system attitude error in the strong vibration environment.

Figs.12 and 13 are the time-varying curves of the output velocity of the inertial navigation system under the vibrations in the x and y directions, respectively. The two subplots represent the easting velocity and northing velocity changes, respectively. It can be seen from Table 5 that under different vibration directions, the velocity error of the system with compensated dynamic coning error is significantly smaller than that of the uncompensated system. It indicates that the modeling method of the dy-

dynamic coning error proposed in this paper can effectively improve the navigation accuracy of the laser SINS in the vibration environment.

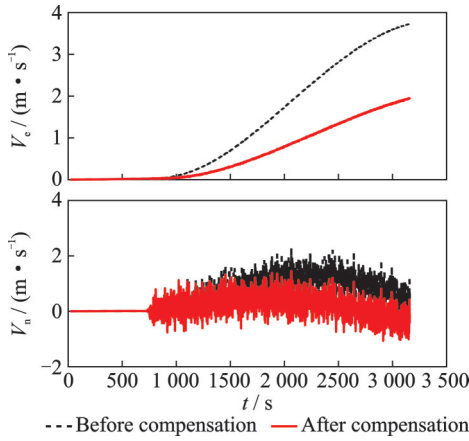


Fig.12 Velocity change curves under x -direction vibration

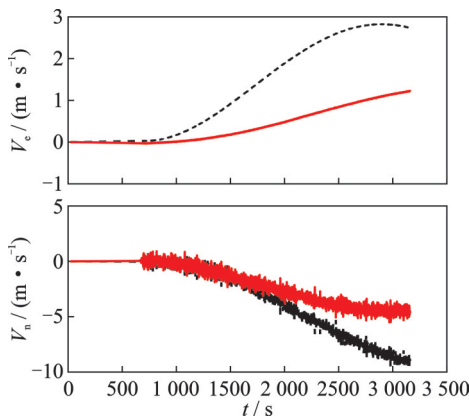


Fig.13 Velocity change curves under y -direction vibration

Table 5 Comparison of maximum velocity errors during vibration process

Velocity	Velocity errors before compensation/($\text{m}\cdot\text{s}^{-1}$)	Velocity errors after compensation/($\text{m}\cdot\text{s}^{-1}$)	Reduction/%
$V_e(x\text{-direction vibration})$	3.83	2.16	43.60
$V_n(x\text{-direction vibration})$	2.27	1.45	36.12
$V_e(y\text{-direction vibration})$	2.83	1.40	50.53
$V_n(y\text{-direction vibration})$	-10.57	-5.51	47.87

4 Conclusions

We propose a method for modeling the dynamic coning error parameters of the laser gyroscope. Firstly, the causes of the dynamic coning error are

analyzed in principle, which is the conical offset of the sensitive axis of the laser gyroscope under the complex mechanical environment. The compensation model of the dynamic coning error is established correspondingly. Then it is proved through the comparative experiment that there exists dynamic coning error compensation effect, and that the existence of the dynamic coning error originates from the system angular acceleration rather than the angular velocity. Finally, through the system-level vibration test, it is verified that the proposed dynamic coning error compensation method can reduce the attitude and speed error of the system in the vibration environment, which can effectively improve the navigation accuracy of the inertial navigation system in the complex mechanical environment.

The current analysis content of this paper is based on the fact that the bending caused by angular acceleration or inertia moment to the gyro sensitive axis is first-order linear. In order to consider the non-linear factors under the large dynamic environment, the model should be further improved based on the high-precision application scenario under the large dynamic environment in the future.

References

- [1] LI J L, FANG J C, GE S S. Kinetics and design of a mechanically dithered ring laser gyroscope position and orientation system[J]. IEEE Transactions on Instrumentation & Measurement, 2013, 62(1): 210-220.
- [2] WANG L, WU W, LI G, et al. Ring laser gyro G-sensitive misalignment calibration in linear vibration environments[J]. Sensors, 2018, 18(2): 601.
- [3] ZHANG Y, WU W Q, ZHANG X Q, et al. Fast and high accuracy initial alignment algorithm for rate biased RLG SINS on stationary base[J]. Systems Engineering and Electronics, 2011, 33(12): 2706-2710.
- [4] YAN G M, WENG J. Strapdown inertial navigation algorithm and integrated navigation principle[M]. Xi'an, China: Northwestern Polytechnical University Press, 2019: 1-36.
- [5] TERCJAK M, BRZEZINSKI A. On the influence of known diurnal and subdiurnal signals in polar motion and UT1 on ring laser gyroscope observations[J]. Pure and Applied Geophysics, 2017, 174(7): 2719-2731.
- [6] ZENG Qinghua, LIU Jianye, ZHAO Wei. Attitude algorithm with incremental angle of RLG SINS[J].

- Journal of Nanjing University of Aeronautics & Astronautics, 2007, 39(2): 143-148. (in Chinese)
- [7] RICHARDSON L W. Ring laser gyro applications for high-accuracy pointing and tracking in space[C]//Proceedings of Acquisition, Tracking, and Pointing VIII. [S.l.]: SPIE, 1994: 101-115.
- [8] REGIMANU B, DAS K C, RAO K S, et al. Dither filtering of real RLG signal using wavelet transforms[J]. Gyroscopy and Navigation, 2019, 10: 275-282.
- [9] CHEN A, LI J, CHU Z. Dither signal removal of ring laser gyro POS based on combined digital filter[C]//Proceedings of 2012 8th IEEE International Symposium on Instrumentation and Control Technology (ISICT). [S.l.]: IEEE, 2012: 178-182.
- [10] WANG K, GU Q. Key problems of mechanically dithered system of RLG[J]. Tsinghua Science and Technology, 2001, 6(4): 304-309.
- [11] XIONG Z, YU X, LONG X. Parametric design for the peak amplitude of a mechanical dithering ring laser gyroscope[J]. International Journal of Applied Electromagnetics and Mechanics, 2016, 51(4): 445-453.
- [12] CHOI W S, KIM C J. Investigation on output variations of ring laser gyroscope in the presence of non-ideal sinusoidal dithering[C]//Proceedings of Interferometry XXI. [S.l.]: SPIE, 2022.
- [13] FAN Z, LUO H, HU S, et al. Research on lock-in correction for mechanical dithered ring laser gyro[J]. Optical Engineering, 2011, 50(3): 034403.
- [14] WANG K D, YAN L, GU Q T. The influence of noise on output of ring laser gyroscope[J]. Sensors and Actuators A: Physical, 2005, 119(1): 75-83.
- [15] ZHANG L, ZHANG T, WANG M, et al. A high-order coning error compensation algorithm under high rate maneuvering[J]. IEEE Sensors Journal, 2019, 20(1): 208-218.
- [16] KIM K J, YU M J, PARK C G. Flexure error analysis of RLG based INS[J]. Journal of Institute of Control, Robotics and Systems, 2006, 12(6): 608-613.
- [17] YU X, WEIG, LONG X, et al. Finite element analysis and optimization of dither mechanism in dithered ring laser gyroscope[J]. International Journal of Precision Engineering and Manufacturing, 2013, 14(3): 415-421.
- [18] WANG L, WU W, PAN X. RLG SINS dynamic error compensation under vibration environments[J]. Gyroscopy and Navigation, 2018, 9: 35-44.
- [19] TU Y, YANG G, CAI Q, et al. Dynamical analysis and experimental verification of deviation angles caused by rubber dampers deformation in high precision mechanically dithered RLG dual-axis RINS[J]. Mechanical Systems and Signal Processing, 2019, 126: 553-567.
- [20] FANG F, ZENG W, LI Z. Coupled dynamic analysis and decoupling optimization method of the laser gyro inertial measurement unit[J]. Sensors, 2019, 20(1): 111.
- [21] PAUL G S. Blazing gyros: The evolution of strapdown inertial navigation technology for aircraft[J]. Journal of Guidance, Control, and Dynamics, 2013, 36(3): 637-655.
- [22] KIM K, PARK C G. Drift error analysis caused by RLG dither axis bending[J]. Sensors and Actuators, 2007, 133(2): 425-430.
- [23] WANG L, WU W Q, PAN X F, et al. Estimation and compensation for dynamic bending error parameters of mechanical dithered RLG sensitive axis[J]. Journal of Chinese Inertial Technology, 2016, 24(6): 828-831.
- [24] WANG L, WU W, PAN X. RLG SINS dynamic error compensation under vibration environments[J]. Gyroscopy and Navigation, 2018, 9(1): 35-44.
- [25] WANG L, WU W, PAN X. Dynamic error compensation and parameter optimization for RLG SINS in vibration environments[C]//Proceedings of 2017 24th Saint Petersburg International Conference on Integrated Navigation Systems (ICINS). [S.l.]: IEEE, 2017: 1-8.
- [26] YAN G M, YANG X K, WENG J, et al. A general numerical method to obtaining optimized coning compensation coefficients for strapdown attitude algorithm[J]. Journal of Navigation and Positioning, 2017, 5(3): 1-4,23.
- [27] LI G, WEI G, XIE Y P, et al. Isotropic design method of suspension system of dithered RLG strapdown inertial measurement unit[C]//Proceedings of Advanced Materials Research. Switzerland: Trans Tech Publications Ltd, 2014, 1044: 788-797.
- [28] IGNAGNI M B. Optimal strapdown attitude integration algorithms[J]. Journal of Guidance, Control and Dynamics, 1990, 13(2): 363-369.
- [29] JIANG Y F, LIN Y P. Improved strap-down coning algorithm[J]. IEEE Transaction on Aerospace and Electronic Systems, 1992, 28(2): 484-490.
- [30] MCKERN R, MUSOFF H. Strapdown attitude algorithms from a geometric viewpoint[J]. Journal of Guidance and Control, 1981, 4(5): 657-661.
- [31] CUI M, ZENG J. An improved coning error compen-

sation algorithm[C]//Proceedings of 2021 IEEE International Conference on Mechatronics and Automation (ICMA). [S.l.]: IEEE, 2021: 28-32.

Author Mr. CHENG Guoda received the B.S. and M.S. degrees in navigation, guidance and control from Harbin Industrial University, Harbin, China in 2010 and 2012, respectively. Now, he is a Ph.D. candidate in School of Automation, Northwestern Polytechnical University. His research is focused on the technology and application of inertial navigation and multi-source information fusion.

Author contributions Mr. CHENG Guoda designed the study, compiled the models, conducted the analysis, interpreted the results, and wrote the manuscript. Mr. LIU Cong and Mr. WANG Shengjun contributed to data and model components for the laser strapdown inertial navigation system. Mr. GAO Guangen and Dr. YAN Fei contributed to data for the analysis of results. All authors commented on the manuscript draft and approved the submission.

Competing interest The authors declare no competing interests.

(Production Editor: ZHANG Huangqun)

激光捷联惯性导航系统动态锥动误差建模分析

成果达^{1,2}, 刘 聪², 高关根², 王胜军², 严 飞²

(1. 西北工业大学自动化学院, 西安 710072, 中国; 2. 中国航空工业集团公司西安飞行自动控制研究所, 西安 710076, 中国)

摘要:提出了一种机抖激光陀螺的锥动误差参数建模与补偿方法。首先从机理上分析了锥动误差产生的原因, 利用有限元分析方法给出了在不同外界角加速度输入下激光陀螺敏感轴的变形情况;建立了锥动误差的补偿模型,将锥动误差的影响用锥动误差系数表示,该系数仅和激光陀螺自身相关;设计了锥动误差系数的系统级标定方案,利用圆锥运动前后系统的姿态误差与锥动误差系数的关系完成参数标定。然后通过激光陀螺和光纤陀螺的圆锥运动实验,证明了锥动误差的存在;通过系统级的圆锥运动实验,证明了锥动误差的补偿效果。最后通过系统级的振动试验,验证了本文提出的锥动误差补偿方法能够有效地减小振动环境下系统的姿态和速度误差,对提升惯导系统在复杂力学环境下导航精度有着重要作用。

关键词:机抖激光陀螺;捷联惯性导航系统;锥动误差;误差模型;参数标定